available at www.sciencedirect.com

ScienceDirect

journal homepage: www.elsevier.com/locate/jmbbm

Research paper

Mechanical strength of abalone nacre: Role of the soft organic layer

*Marc André Meyers**, *Albert Yu-Min Lin*, *Po-Yu Chen*, *Julie Muyco*

Department of Mechanical and Aerospace Engineering, Materials Science and Engineering Programme, University of California, San Diego, La Jolla, CA 92093-0411, USA

ARTICLE INFO

Article history:
Received 31 January 2007
Received in revised form
7 March 2007
Accepted 8 March 2007
Published online 29 May 2007

ABSTRACT

The nacreous portion of the abalone shell is composed of calcium carbonate crystals interleaved with layers of viscoelastic proteins. The resulting structure yields unique mechanical properties. In this study, we focus on the thin viscoelastic layers between the tiles and on their role on the mechanical properties of the shell. Both SEM and AFM show that the thin (~30 nm) organic layer is porous, containing holes with diameter of approximately 50 nm. These holes enable the formation of mineral bridges between adjacent tile layers. The mineral bridges play a pivotal role in growth and ensure the maintenance of the same crystallographic relationship through tile growth in the 'terraced cone' mode. The existence of mineral bridges is consistent with the difference between tensile and compressive strength of the abalone. Mechanical tests with loading applied perpendicular to the plane of the organic layers reveal a tensile strength lower than 10 MPa, whereas the compressive strength is approximately 300–500 MPa. These nanoscale bridges have, by virtue of their dimensions (50 nm diameter × 30 nm length), a strength that reaches their theoretical value. The calculated tensile strength based on the theoretical strength predicts a bridge density of approximately 2.25/μm².

A major conclusion of this investigation is that the role of the organic layer is primarily to subdivide the $CaCO_3$ matrix into platelets with thickness of 0.5 μm. Its intrinsic effect in providing a glue between adjacent tiles may not be significant.

1. Introduction

The abalone shell has two layers: an outer prismatic layer (rhombohedral calcite) and an inner nacreous layer (orthorhombic aragonite). Aragonitic $CaCO_3$ constitutes the inorganic component of the nacreous ceramic/organic composite (95 wt% ceramic, 5 wt% organic material). This composite comprises stacked platelets (~0.5 μm thick), arranged in a 'brick-and-mortar' microstructure with an organic matrix (20–50 nm thick) interlayer that is traditionally considered as serving as glue between the single platelets. There is a very high degree of crystallographic texture characterized by a nearly perfect "c-axis" alignment normal to the plane of the tiles. As a result of its highly ordered hierarchical structure (Laraia and Heuer, 1989; Vincent, 1991; Baer et al., 1992; Srinivasan et al., 1991; Heuer et al., 1992; Sarikaya, 1994; Mayer and Sarikaya, 2002), the nacreous layer exhibits excellent mechanical properties.

* *Corresponding author.* Tel.: +1 858 534 4719; fax: +1 858 534 5698.
E-mail address: mameyers@ucsd.edu (M.A. Meyers).

1751-6161/$ - see front matter © 2007 Elsevier Ltd. All rights reserved.
doi:10.1016/j.jmbbm.2007.03.001

There is a second element to the hierarchy: growth bands, or mesolayers. Layers of organic material with a thickness of about 20 μm separate the thicker mesolayers which are approximately 300 μm thick. These layers were identified by Menig et al. (2000), Su et al. (2002), and Lin and Meyers (2005) but are not often mentioned in other reports dealing with the mechanical properties of abalone. It is thought that these thick organic layers form in abalone grown in the sea during periods in which there is little growth.

Fig. 1a shows the inside surface (nacreous) of an abalone shell. The cross-section shows the mesolayers, which are spaced approximately 300 μm apart and are separated by thick regions that consist of primarily organic material with minerals embedded into it (Lin et al., 2006). The mineral regions are comprised of the tiles discussed above; they are separated by the organic nanolayers. The effectiveness of this structure in increasing the toughness is demonstrated by the SEM micrograph of the tiles being pulled apart in a fracture region (lower left-hand side of Fig. 1a).

Currey (1977) was the first to perform measurements of mechanical properties of nacre from a variety of bivalves, gastropods and cephalopods. He obtained a fracture strength in bending varying between 56 and 116 MPa. This was followed by Jackson et al. (1988) who used nacre from the shell of a bivalve mollusk, *Pinctada*. They reported a Young's modulus of approximately 70 GPa for dry and 60 GPa for wet samples; the tensile strength of nacre was found to be 170 MPa for dry and 140 MPa for wet samples. The work of fracture varied from 350 to 1240 J/m^2, depending on the span-to-depth ratio and the degree of hydration, wet nacre showing superior toughness by associated introduction of plastic work. In contrast, monolithic $CaCO_3$ showed a work of fracture that was up to 3000 times less than that of the composite nacre material. The work-of-fracture is the area under the stress–strain curve and is deeply affected by gradual, graceful fracture, whereas the fracture toughness does not incorporate this entire process.

Mechanical tests on red abalone (*Haliotis rufescens*) were conducted by Sarikaya et al. (1990), Sarikaya and Aksay (1992), and Sarikaya (1994) and a fracture strength of 185 ± 20 MPa (in bending tests) and a fracture toughness of 8 ± 3 MPa $m^{1/2}$ were obtained. This latter value is an eight-fold increase in toughness over monolithic $CaCO_3$. The scatter was explained by the natural defects in the nacre and the somewhat curved shape of the layers. Menig et al. (2000) applied Weibull statistics (Weibull, 1951) and successfully explained the variation. They obtained mean tensile strengths of 177 and 197 MPa for flexure testing parallel and perpendicular to the surface plane, respectively. These results are in full agreement with Jackson et al. (1988), Sarikaya et al. (1990), Sarikaya and Aksay (1992), and Sarikaya (1994). Wang et al. (2001) also determined the flexural tensile strength of red abalone (*H. rufescens*) and obtained values of 194 and 223 MPa for loading (in flexure) parallel and perpendicular to the surface plane. The compressive strength obtained by Menig et al. (2000), on the other hand, was much higher and equal to 540 and 235 MPa for loading perpendicular and parallel to the layered structures. The low value obtained in the parallel direction was attributed to the observation of microplastic buckling (Menig et al., 2000). Thus, the ratio between compressive and tensile strength is in the range 1.5–3, in contrast with the conventional monolithic ceramics, in which it is 8–15.

Several toughening mechanisms have been proposed by Sarikaya et al. (1990), and Sarikaya and Aksay (1992): (a) crack blunting/branching/deflection, (b) microcrack formation, (c) plate pull out, (d) crack bridging (ligament formation). The high degree of crack tortuosity in these shells may be due mainly to crack blunting and branching. Menig et al. (2000) also observed crack deflection at the mesolayers, which have thick (20 μm) organic interfaces. Additional toughening mechanisms such as sliding of $CaCO_3$ layers and organic ligament formation were thought to operate and were analysed by Lin and Meyers (2005). Evans et al. (2001) and Wang et al. (2001) proposed an alternative toughening mechanism: that nano-asperities on the aragonite tiles are responsible for the mechanical strength. These nano-asperities create frictional resistance to sliding, in a manner analogous to rough fibers in composite material. They developed a mechanism that predicts the tensile mechanical strength based on these irregularities. These nano-asperities were modelled by Barthelat et al. (2006), who carried out nanoindentation and FEM analysis of the aragonite crystals. Bruet et al. (2005) obtained, through nanoindentation and atomic force microscopy, local measurements of the mechanical properties of the aragonitic tiles: $E = 79$ and 92 GPa and compressive strengths of 11 and nine GPa for dry and seawater soaked tiles, respectively.

The growth of the abalone shell has been the subject of considerable past study. The work by the UC Santa Barbara group (Fritz et al., 1994; Zaremba et al., 1996; Belcher, 1997; Belcher et al., 1996, 1998; Belcher and Gooch, 2000; Shen et al., 1997; Fritz and Morse, 1998) represents the most comprehensive effort. The study whose results are presented here is not concerned about the molecular structure of the organic layer, but with the role of that layer in the overall mechanical response of nacre.

2. Experimental methods

A new method ('trepanning') was used for the observation of growth mechanisms in nacre. It consists of (a) coring out a cylindrical section of the abalone shell, (b) replacing by one with slightly larger diameter, and (c) removing at regular intervals to observe the restart of growth. It was supplemented by the Santa Barbara flat pearl technique (Fritz et al., 1994), which has been used previously by Lin and Meyers (2005).

Both a FEI environmental SEM (Scripps Institute of Oceanography) and a FEI field emission SEM were used for characterization with accelerating voltages of 15–20 kV. Samples were examined immediately after removal in order to maintain hydration of the organic matrix. Before examination, the slides and cylinders are usually washed in purified water to remove salt build up. However, for observation of the organic layer the washing procedure was eliminated to preserve the organic growth material. The AFM characterization on the organic layer was carried out at Lawrence Livermore National Laboratory. The organic

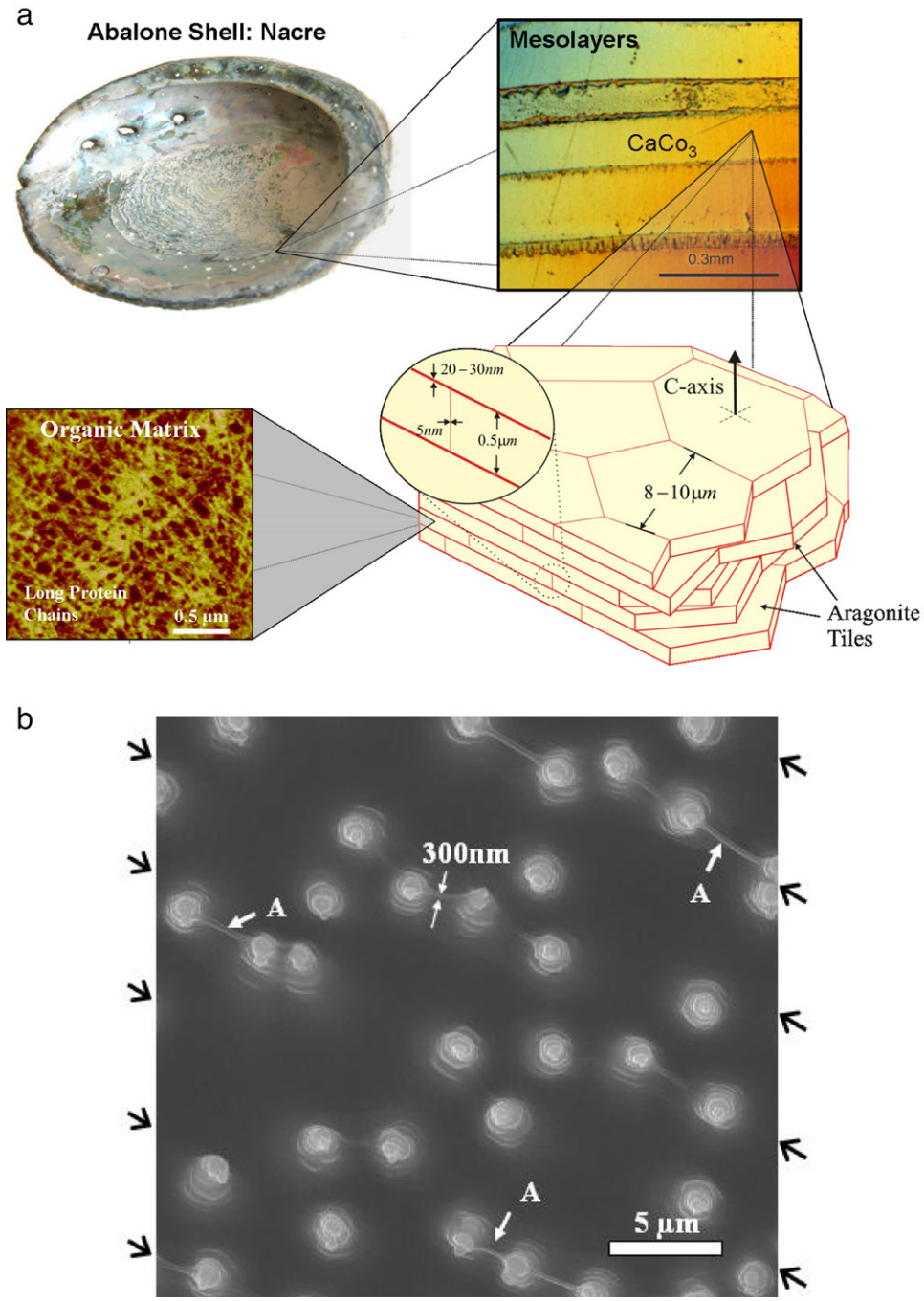

Fig. 1 – (a) Overall view of hierarchical structure of abalone shell, showing mesolayers, mineral tiles, and tile pullout in a fracture region. (b) Top growth surface six weeks after implantation. Light regions represent apexes of terraced cones and streaks marked by arrows are due to folding of organic interlayer.

layers were separated from the aragonite tiles by EDTA demineralization. Strips of the organic nanolayers were kept in a saline solution until observation by AFM.

The abalone (both red and green) were held at the Scripps Institution of Oceanography, in open system tanks in which continuous fresh sea water (removed circulation) was provided. They were fed kelp (*Macrocystis pyrifera*) on a regular schedule. The specimens were removed at one week intervals at times up to six weeks.

Mechanical testing was carried out in tension and compression. The direction of both tensile and compression loads was perpendicular to the large dimension of the tiles, corresponding to the surface of the shell. For tensile testing the specimens were extracted using a coring drill. They had a diameter of 3 mm. The calcite layer was ground away until the entire thickness consisted exclusively of aragonite tiles. Two methods were used for tensile testing of the nacre with loading perpendicular to the plane of the tiles. The upper and lower surfaces of the specimens were glued to aluminum holders and allowed to cure for 24 h with the loading

assembly in place. The assembly was either mounted in an Instron testing machine or at the extremity of a cantilever beam so that no bending was applied to the specimen. The breaking load was determined and the surfaces characterized by SEM. The compression specimens were obtained through two techniques: (a) cutting cubes from the shell using a high speed diamond blade (Menig et al., 2000); (b) cylindrical specimens prepared as described above.

3. Results and discussion

3.1. *Growth arrest experiments*

The top view of the growth surface after six weeks is shown in Fig. 1b. The terraced cones can be seen, albeit not too clearly, because they are covered by an organic layer. The tips of the terraced cones (which we call Christmas trees) are the lighter features, with a separation of 5–10 μm, corresponding to the steady state tile diameter. Parallel lines (marked by arrows) connect the tips of some cones. These parallel lines are oriented at ~30° to the horizontal axis of Fig. 1b. They correspond to the folding of the organic layer. These folds, three of which are marked by arrows A, have a thickness of approximately 300 nm. The effect is analogous to the folds formed on top of tents. Previous observation (Lin and Meyers, 2005) of the growth surface after cleaning by water did not reveal the organic layer. It is thought that even small perturbations can remove this layer.

The growth sample was fractured in tension parallel to the growth surface to enable a lateral observation of the structure along the *a* and *b* direction of growth. This was done after the structure was allowed to dry. The results are shown in Fig. 2a. The structure is remarkably well retained. The top corresponds to the growth surface and the bottom to the fully interweaved tiles. The tips of the terraced cones protrude through the top layer of the organic material. In places, such as that which is marked with an arrow B, the organic material is ruptured. This is presumably due to the drying process. The folding of the organic membrane is also seen and is marked by arrow A. Again, the features on the top three mineral layers of the terraced cones are not clear because they are covered by the organic layer. Fig. 2b is a schematic showing the sagging of the membrane under its own weight.

Upon closer observation, the organic layer stretched between tiles is seen to contain rings of holes (Fig. 3a). This is in contrast with the top (growth) layer, which does not show these holes (Fig. 1b and 2a). These holes are produced by the stretching introduced during the fracturing process. The holes have diameters which increase with the stretch. Similar holes were also observed by Belcher and Gooch (2000) (Figs. 15.1 and 15.9). These observations suggest that existing holes expand upon stretching of the organic membrane. Fig. 3b shows, in schematic fashion, an initially random pattern of holes. Upon stretching the membrane biaxially, the circumferential stresses at the edges of the holes experience twice the applied stresses. Thus, the strain along them is higher than the overall strain and the rate of growth of the holes is larger than the overall strain (Fig. 3c). This

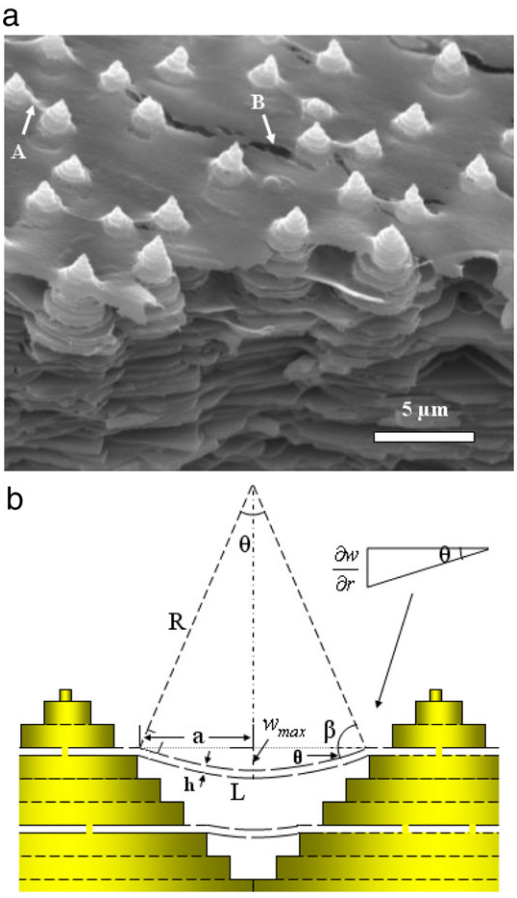

Fig. 2 – (a) Side view of intermediate tile growth through organic layers on flat pearl five weeks after implantation. (b) Schematic showing terraced growth and organic membrane sagging under its own weight.

explains the presence of large holes (up to 400 nm) in severely stretched layers.

Atomic force microscopy on the organic layer revealed the outline of the tiles (Fig. 4a). One of the tiles is schematically shown, for clarity. It should be mentioned that the material was completely demineralized. This outline is due to variations of morphology and thickness associated with the tile boundaries. Higher magnification observation in the tapping mode revealed the detailed structure of the organic layer (Fig. 4b). There are two principal components: long (Lustrin protein?) chains arranged in a random pattern; holes with diameter 20–50 nm. The depth of the holes can be gauged from the depth scale in the right-hand side of Fig. 4b. The surface corresponds to 30 nm, and the holes correspond to the baseline of the depth scale.

3.2. *Calculation of organic nanolayer stiffness from deflection*

The sagging of the organic layer, shown in Fig. 1b and 2a, can be used to estimate its stiffness. The fact that the organic membrane undergoes substantial sagging from the sole effect of its weight suggests that its stiffness is very low. The sagging of a membrane is a classical mechanics problem. We present

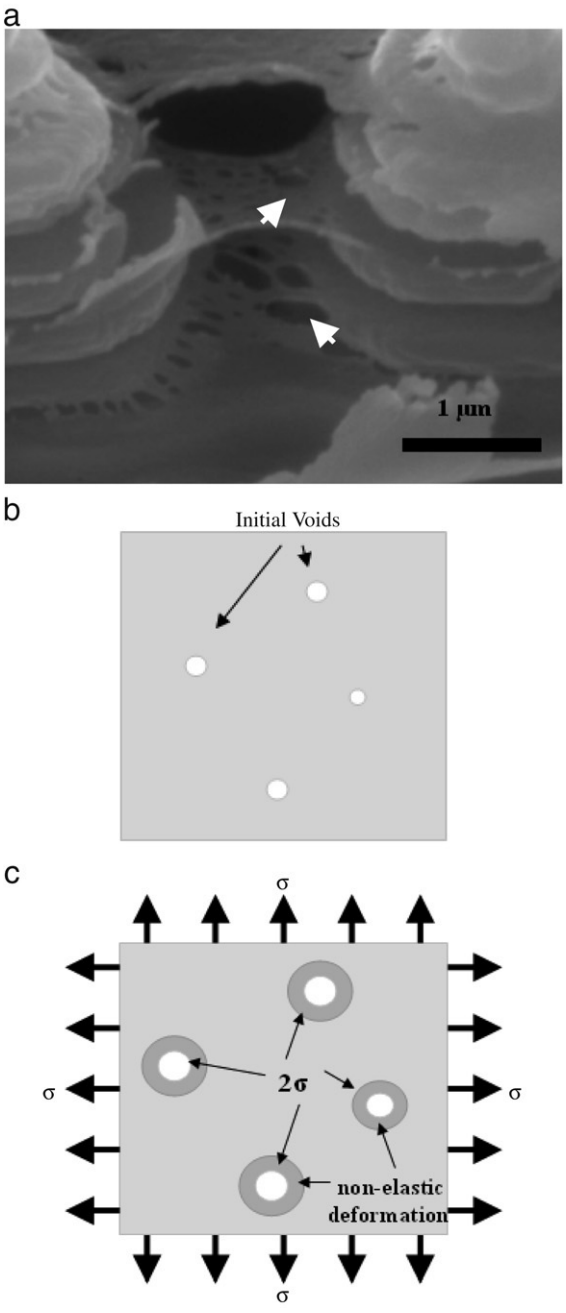

Fig. 3 – (a) SEM of membranes with holes that formed upon stretching; (b) schematic representation of membrane with holes; (c) membrane subjected to biaxial stress.

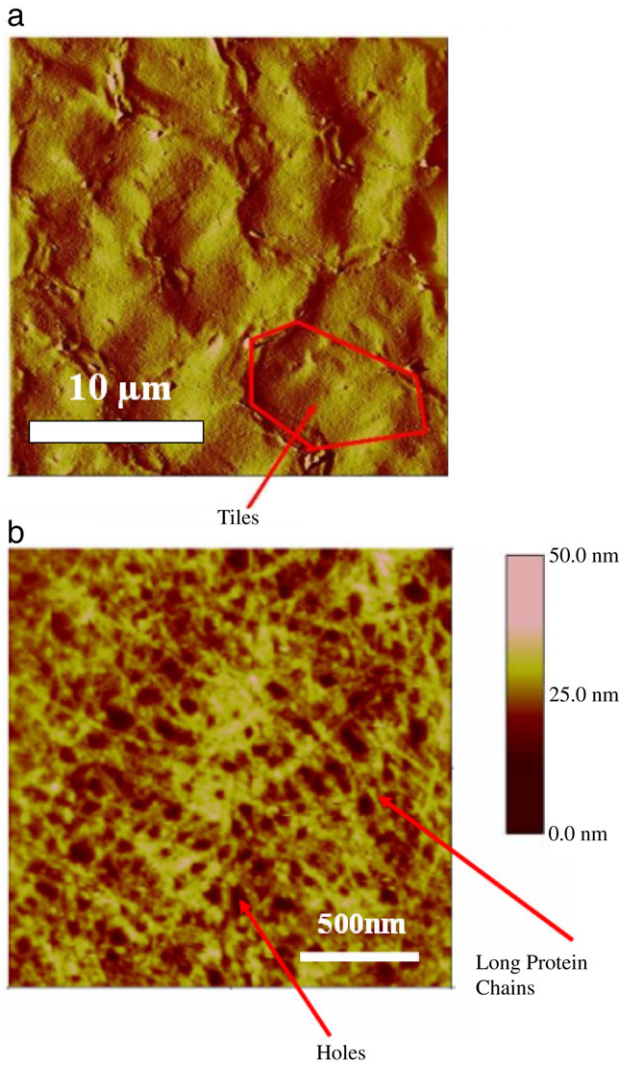

Fig. 4 – Atomic force microscopy of organic layer; (a) overall view at low magnification showing outline of hexagonal tiles; (b) high magnification showing linear chains and holes with ~30 nm diameter.

here a solution applicable to the simple boundary conditions. The membrane is assumed to be circular and fixed along the circle. Its deflection as a result of its weight is calculated. The radial forces are considered to be zero at zero deflection. The equilibrium diagram is shown in Fig. 2b. The following parameters are defined: a, radius of the membrane (assumed to be circular); w, deflection; h, thickness of the membrane; σ, radial stress on membrane. One finds that w_{max}, the maximum deflection, can be expressed in terms of known parameters (e.g. Ugural (1981), Szilard (2004)):

$$w_{max} = \frac{\rho h g a^2}{4N} \tag{1}$$

ρ is the density; N is the tensile force per unit length which is represented by stress multiplied by unit thickness:

$$N = \sigma h. \tag{2}$$

The biaxial stress in a membrane under its own weight is

$$\sigma = \frac{\rho g a^2}{4 w_{max}}. \tag{3}$$

The nominal biaxial strain is defined as

$$\varepsilon = \frac{L - 2a}{2a}. \tag{4}$$

For the calculation of the strain, we assume θ, the angle between the a–b plane of growth and the outer edges of the sagging membrane, is small. Thus

$$\sin\theta \cong \tan\theta = \frac{\partial w}{\partial r} = \frac{w_{max}}{a} \tag{5}$$

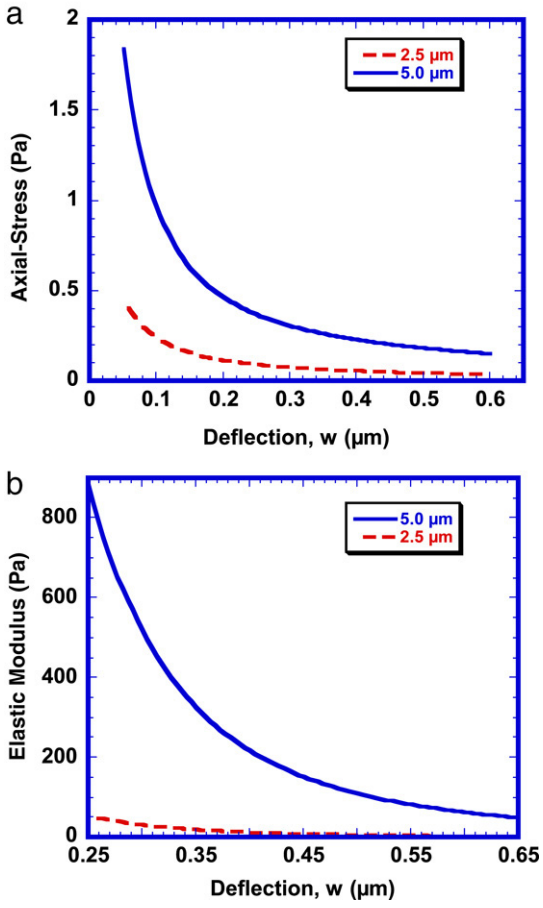

Fig. 5 – Calculated (a) stress, and (b) elastic modulus of organic layer as a function of deflection for two circle radii (assumed shape between sagging points of the membrane) are considered: 2.5 and 5 μm.

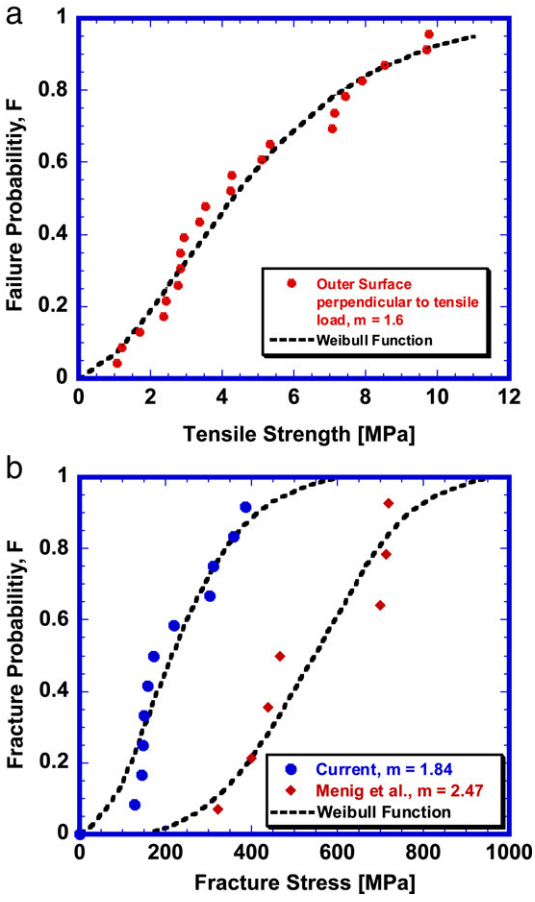

Fig. 6 – Weibull distribution of (a) tensile and (b) compressive strengths with force direction perpendicular to layered structure.

$$L = 2\pi R\frac{\theta}{180^\circ} = 2\pi\frac{a^2}{w_{\max}}\frac{\theta}{180^\circ}. \quad (6)$$

We assume the density of the organic layer to be 1.5 g/cm^3. The thickness of the membrane is taken to be 30 nm, in accordance with several measurements reported in the literature and our own approximate evaluation. Two circle radii (assumed shape between sagging points of the membrane) are considered: 2.5 and 5 μm. This is consistent with tile size of approximately 5–10 μm. Fig. 5a shows the stresses calculated using Eq. (3). The deflection, average distance between the lowest point of the membrane and the *a*–*b* plane of growth, is varied from zero to 0.6 μm. The corresponding biaxial modulus, obtained by dividing Eq. (3) by (4), is plotted in Fig. 5b. Although this is difficult to evaluate, the deflection can be estimated from Fig. 2a. This deflection varied somewhat and there are uncertainties that are beyond the measure. One could argue that the dried membrane has properties different from the original hydrated membrane. However, it is thought that the drying process 'freezes in' the existing configuration. Many other observations confirm the extreme 'softness' of the layer, as well as its poor adherence to the tiles. Taking a value of 0.5 μm, consistent with the sagging shown in Fig. 2, one obtains a biaxial elastic modulus of 100 Pa, considering a tile spacing of 10 μm ($a = 5$ μm). This is indeed a very low value. This low value can only be explained if the random network of protein chains in Fig. 4b can slide when tension is applied to the membrane. The value of 100 Pa is an upper bound, and the range of elastic moduli is comparable to that of other living cells (Bao and Suresh, 2003). This value is also consistent with the high maximum tensile strains that the organic layer can undergo in tension. Belcher and Gooch (2000) (Fig. 15.9) quote a value of $\varepsilon_{\max} = 3$ (equivalent to a maximum stretch $\lambda = \varepsilon + 1 = 4$). The calculations confirm that the organic layer material has a very small stiffness.

3.3. *Mechanical tests perpendicular to layer plane*

As discussed in the introduction, there have been a considerable number of studies determining both compressive and tensile strength along the tile plane (loading axis parallel to shell surface). The determination of the shell strength when the loading is applied perpendicular to its surface can directly address the role played by the organic layer. The results, expressed as Weibull plots, are shown in Fig. 6a. For comparison, the compressive strength in the same orientation is

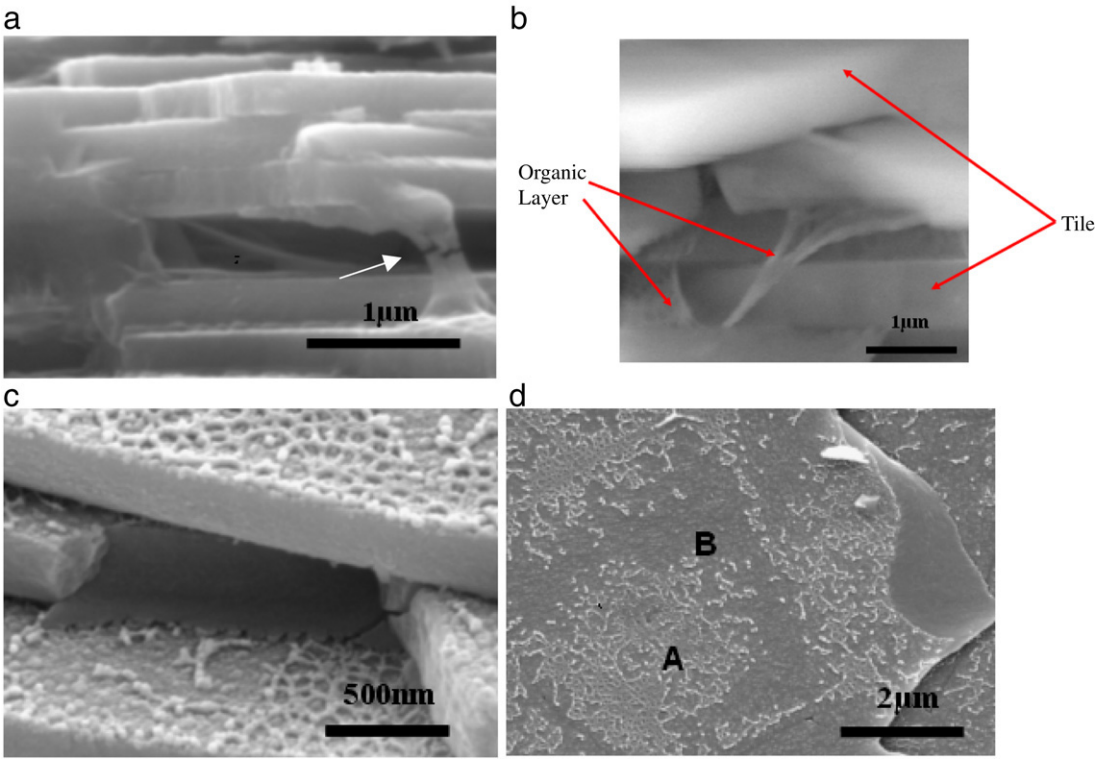

Fig. 7 – Various views of organic layer in specimen subjected to tensile test (field-emission SEM); (a, b) layers hanging between two tiles (marked with arrow); (c, d) top view of tile surface with organic layer networks.

shown in Fig. 6b. The same distribution was observed previously in abalone and conch (Menig et al., 2000, 2001) shells. The Weibull moduli in both tension and compression are similar: 1.6 and 1.8–2.5, respectively, as seen in Fig. 6a and b, respectively. However, the difference in strength is dramatic and much greater than in conventional brittle materials. The ratio between compressive and tensile strength is of the order of 50, whereas brittle materials it varies between 8 and 12. This difference is indeed striking, especially if one considers the tensile strength parallel to the layer plane; it is on the order of 150–200 MPa, one third of the compressive strength. It should be mentioned that in composites this ratio in the fiber direction is much more favourable; in this sense, the nacreous portion of the shell can be considered a composite. This was discussed by Menig et al. (2000). It can be concluded that the shell sacrifices tensile strength in the perpendicular direction to the tiles to use it in the parallel direction. Interestingly, the average of the tensile strength (in the perpendicular and parallel directions) is approximately 75–100 MPa, whereas the compressive strength is approximately 500 MPa. This is much closer to the 'normal' value for the ratio between compressive and tensile strength of ceramics.

SEM characterization of the surfaces fractured in tension reveals the failure path. For the most part, it occurs in the inter-tile regions. Fig. 7a and b show fractured regions with partial separation between tiles. Thin sections of the organic layer, hanging between adjacent tile layers, are seen. Although the detailed features could not be resolved, it is clear that the organic layer is very soft. It is also apparent that it is not firmly attached to the tiles. The field-emission SEM enabled a resolution of down to 10 nm. Fig. 7c and d show the top surfaces of tiles. Irregular features, the remnants of the organic layer, can be seen attached to these mineral surfaces. In Fig. 7d some regions (marked A) show the fabric of the organic layer, where other regions (marked B) are characteristic of the mineral. The organic material appears to have a fishnet structure, with a substantial fraction of holes. These holes have a diameter of approximately 50 nm, consistent with the AFM observations. The lateral surfaces of the tiles are much smoother than the top and bottom surfaces. This is seen more clearly in Fig. 8. Two features are evident:

1. The presence of a large number of asperities with approximate diameter of 50 nm and slightly smaller height (~30 nm). The diameter of the asperities is consistent with the sizes of the holes in the organic layer;
2. The existence of mineral bridges between adjacent tile layers (arrows, Fig. 8b). Mineral bridges were first suggested by Belcher (1997) and identified by Schäffer et al. (1997) and Song et al. (2002, 2003). Barthelat et al. (2006) provide clear TEM evidence for both mineral bridges and asperities. The bridge mechanism explains why the crystalline structure between successive tiles from a same terraced cone (Christmas tree) growth is retained. Indeed, Lin and Meyers (2005) pointed out that the parallelism in the facets of the hexagonal tiles on a same terraced cones suggested a same crystalline orientation.

Three models for the inter-tile region are shown in Fig. 9. The asperity model by Wang et al. (2001) and Evans et al. (2001) is represented in Fig. 9a. The tensile strength in the

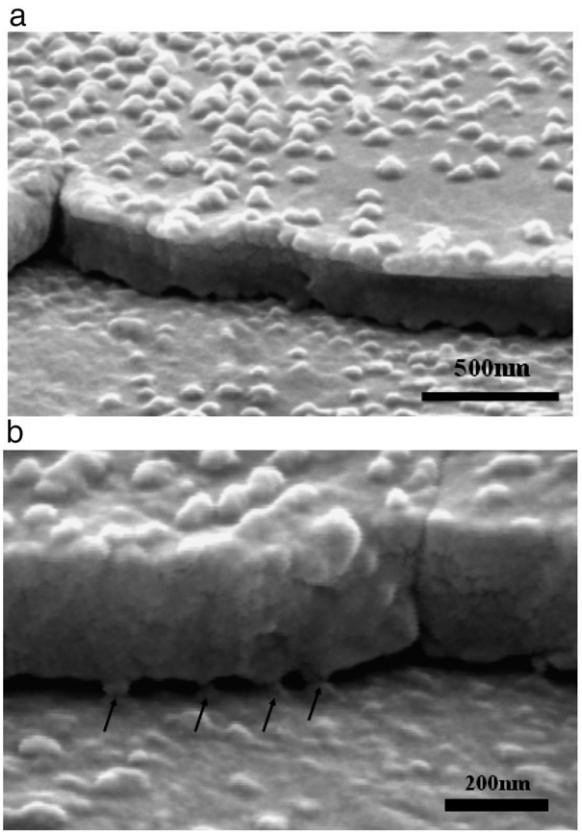

Fig. 8 – (a) Asperities (a fraction of which are remnants of mineral bridges) and (b) mineral bridges (marked by arrows) between tile layers.

layered plane was explained by them as due to the frictional resistance of the asperities to the sliding of the tiles. Evans et al. (2001) pointed out that the organic layer provides the glue between adjacent tiles, enabling the frictional mechanism to operate. Fig. 9b shows the viscoelastic glue model according to which the tensile strength is the result of stretching of molecular chains whose ends are attached to surfaces of adjacent tiles. Fig. 9c shows the mineral bridge model, consistent with our observations. The sliding of adjacent tiles requires the breaking of bridges and the subsequent frictional resistance, in a mode akin to the Wang et al. (2001) and Evans et al. (2001) mechanism.

3.4. *Calculation of tensile strength*

One can estimate the tensile strength of the individual mineral bridges. Consistent with recent analyses by Gao et al. (2003), Ji and Gao (2004) and Ji et al. (2004), the mineral bridges have sizes in the nanometer range. We start by applying the fracture mechanics equation to aragonite. The maximum stress, σ_{fr}, as a function of flaw size, $2a$, can be estimated, to a first approximation, to be

$$\sigma_{fr} = \frac{K_{Ic}}{\sqrt{\pi a}} \tag{7}$$

where K_{Ic} is the fracture toughness. However, the strength is also limited by the theoretical tensile strength, which can be approximated as (Gao et al., 2003)

$$\sigma_{th} = \frac{E}{30}. \tag{8}$$

We assume that $K_{Ic} = 1$ MPa $m^{1/2}$, $E = 100$ GPa, and that $2a = D$, where D is the specimen diameter. Fig. 10a shows the two curves given by Eqs. (7) and (8). They intersect for $a = 28$ nm ($D = 56$ nm). This is indeed surprising, and shows that specimens of this and lower diameter can reach the theoretical strength. This is in agreement with the experimental results: the holes in the organic layer and asperities/bridge diameters are around 50 nm. Recent analyses (Song et al., 2002, 2003; Gao et al., 2003) also arrive at similar values.

It is possible to calculate the fraction of the tile surface consisting of mineral bridges, f. Knowing that the tensile

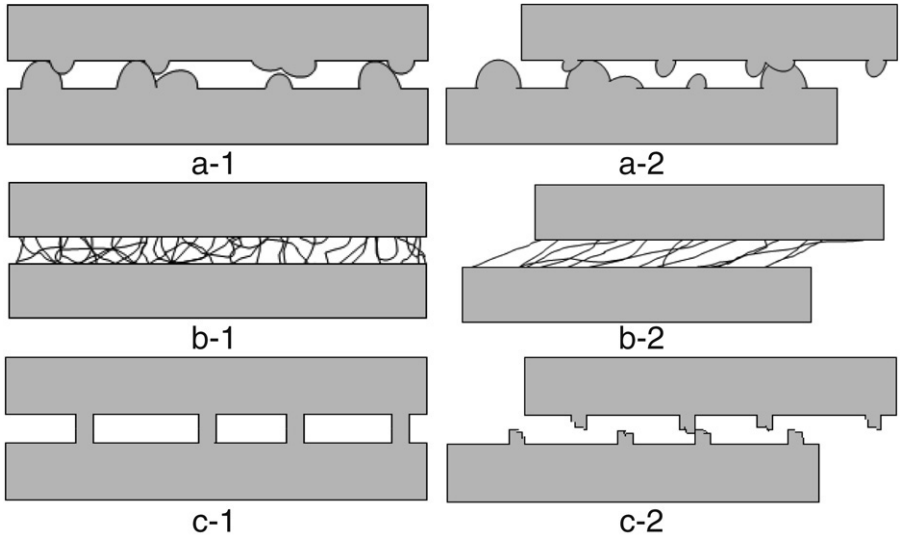

Fig. 9 – Different models for sliding between tiles; intertile layer formed by (a) asperities; (b) organic layer acting as viscoelastic glue; (c) mineral bridges.

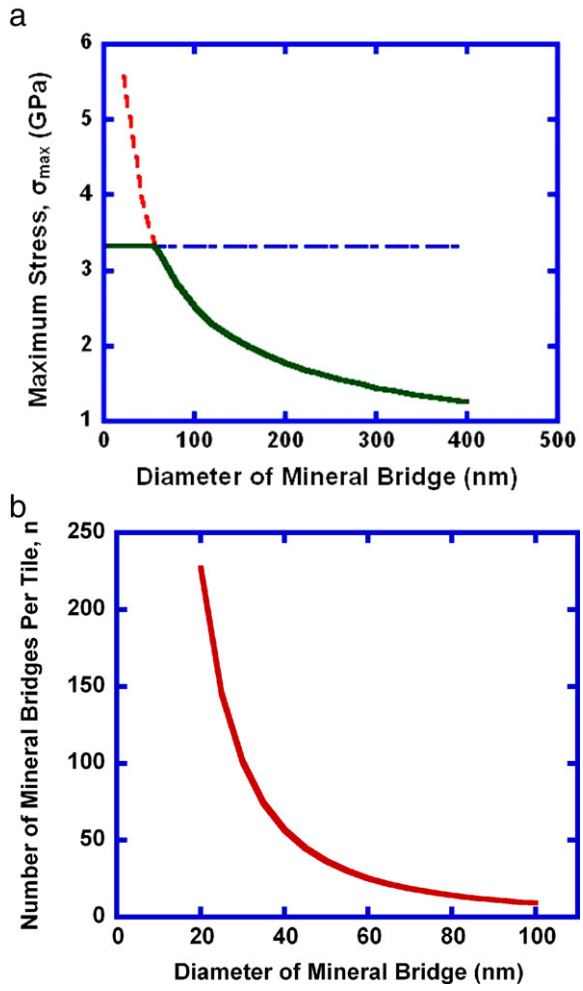

Fig. 10 – (a) Tensile strength of mineral as a function of size; (b) calculated number of mineral bridges per tile as a function of bridge diameter.

strength is σ_t and assuming that the bridges fail at σ_{th}, we have

$$f = \frac{\sigma_t}{\sigma_{th}}. \quad (9)$$

The number of bridges per tile, n, can be calculated from

$$f = \frac{nA_B}{A_T} \quad (10)$$

where A_B is the cross-sectional area of each bridge and A_T is the area of a tile. Thus

$$n = \frac{\sigma_t A_T}{\sigma_{th} A_B}. \quad (11)$$

Assuming that the tiles have a diameter of 10 μm and that the bridges have a diameter of 50 nm (the approximate observed value), one obtains, for $\sigma_t = 3$ MPa (the value at $F = 0.5$ in Fig. 6a) and $\sigma_{th} = 3.3$ GPa, $n = 36$. This corresponds to a bridge density of 2.25/μm^2.

The number of asperities seen in Fig. 8 exceeds considerably the values for bridges calculated herein. From the image the estimated density is 60/μm^2. Song et al. (2001, 2002) had determined an average density of 105/μm^2, which is in agreement with the results by Schäffer et al. (1997) who reported a hole density of 97/μm^2. This is consistent with the present measuerments. One conclusion that can be drawn is that a large number of asperities are indeed incomplete bridges and that these bridges are a small but important fraction of the protuberances.

4. Conclusions

The observations made herein indicate that the organic layer, while playing a pivotal role in the growth of the aragonite crystals in the c direction (perpendicular to tile surface), may have a minor role in the mechanical strength. The tensile strength in the direction perpendicular to the layered structure can be explained by the presence of the mineral bridges. These bridges, having a diameter of approximately 50 nm, have a tensile strength no longer determined by the critical crack size, but by the theoretical strength. Their number is such that the tensile strength of the tiles (parallel to the tile/shell surface plane) is optimized for the tile thickness of 0.5 μm, as shown by Lin and Meyers (2005). A higher number of bridges would result in tensile fracture of the tiles with loss of the crack deflection mechanism. This is a viable explanation for the small fraction of asperities that are bridges.

It is concluded that the scale of the structural components in nacre is an important parameter. Efforts at mimicking these biological composites have to incorporate the scale to derive the full benefit of these hierarchical designs (Mayer, 2005). Indeed, abalone is inspiring scientists in the synthesis of novel materials as evidenced by a recent report (Deville et al., 2006).

Acknowledgements

We are immensely grateful to Evelyn York, SIO, and Ryan Anderson, Calit2, for helping us with SEM. Mr E. Kisfaludy, SIO, helped us with the feeding and welfare of the abalone. This research is supported by the National Science Foundation DMR Grant 0510138. We thank Drs Linnette Madsen and Joseph Akkara for support and encouragement. Dr Chris Orme, Lawrence Livermore National Laboratory, graciously allowed us to use the AFM facilities and hosted us during our visits. Discussions with Profs R.J. Asaro and J.M. McKittrick are gratefully acknowledged.

REFERENCES

Baer, E., Hiltner, A., Morgan, R.J., 1992. Biological and synthetic hierarchical composites. Phys. Today 45, 60–67.

Bao, G., Suresh, S., 2003. Cell and molecular mechanics of biological materials. Nat. Mat. 2, 715–725.

Barthelat, F., Li, C.M., Comi, C., Espinosa, H.D., 2006. Mechanical properties of nacre constituents and their impact on mechanical performance. J. Mater. Res. 21, 1977–1986.

Belcher, A.M., Gooch, E.E., 2000. In: Bauerlein, E. (Ed.), Biomineralization: From Biology to Biotechnology and Medical Application. Wiley-Interscience, Germany, p. 221.

Belcher, A.M., Hansma, P.K., Stucky, G.D., Morse, D.E., 1998. First steps in harnessing the potential of biomineralization as a route to new high-performance composite materials. Acta Mater. 46, 733–736.

Belcher, A.M., Wu, X.H., Christensen, R.J., Hansma, P.K., Stucky, G.D., Morse, D.E., 1996. Control of crystal phase switching and orientation by soluble mollusk shell proteins. Nature 381, 56–58.

Belcher, A.M., 1997. Spatial and temporal resolution of interfaces, phase transitions and isolation of three families of proteins in calcium carbonate based biocomposite materials. Ph.D. Thesis. U. California, Santa Barbara.

Bruet, B.J.F., Qi, H.J., Boyce, M.C., Panas, R., Tai, K., Frick, L., Ortiz, C., 2005. Nanoscale morphology and indentation of individual nacre tablets from the gastropod mollusc Trochus niloticus. J. Mater. Res. 20, 2400–2419.

Currey, J.D., 1977. Mechanical properties of mother of pearl in tension. Proc. R. Soc. Lond. 196, 443–463.

Deville, S., Saiz, E., Nalla, R.K., Tomsia, A.P., 2006. Freezing as a path to build complex composites. Science 311, 515–518.

Evans, A.G., Suo, Z., Wang, R.Z., Aksay, I.A., He, M.Y., Hutchinson, J.W., 2001. Model for the robust mechanical behavior of nacre. J. Mater. Res. 16, 2475–2484.

Fritz, M., Belcher, A.M., Radmacher, M., Walters, D.A., Hansma, K., Stucky, G.D., Morse, D.E., 1994. Flat pearls from biofabrication of organized composites on inorganic substrates. Nature 371, 49–51.

Fritz, M., Morse, D.E., 1998. The formation of highly organized biogenic polymer/ceramic composite materials: The high-performance microaluminate of molluscan nacre. Col. Iner. Sci. 3, 55–62.

Gao, H.J., Ji, B.H., Jäger, I.L., Arzt, E., Fratzl, P., 2003. Materials become insensitive to flaws at nanoscale: Lessons from nature. Proc. Natl. Acad. Sci. USA 100, 5597–5600.

Heuer, A.H., Fink, D.J., Laraia, V.J., Arias, J.L., Calvert, P.D., Kendall, K., Messing, G.L., Blackwell, J., Rieke, P.C., Thomson, D.H., Wheeler, A.P., Veis, A., Caplan, A.I., 1992. Innovative materials processing strategies: A biomimetic approach. Science 255, 1098–1105.

Jackson, A.P., Vincent, J.F.V., Turner, R.M., 1988. The mechanical design of nacre. Proc. R. Soc. Lond. B 234, 415.

Ji, B.H., Gao, H.J., Hsia, K.J., 2004. How do slender mineral crystals resist buckling in biological materials. Philos. Mag. Lett. 84, 631–641.

Ji, B.H., Gao, H.J., 2004. Mechanical properties of nanostructure of biological materials. J. Mech. Phys. Solids 52, 1963–1990.

Laraia, J.V., Heuer, A.H., 1989. Novel composite microstructure and mechanical behavior of mollusk shell. J. Am. Ceram. Soc. 72, 2177–2179.

Lin, A., Meyers, M.A., 2005. Growth and structure in abalone shell. Mater. Sci. Eng. A 390, 27–41.

Lin, A.Y.M., Meyers, M.A., Vecchio, K.S., 2006. Mechanical properties and structure of Strombus gigas, Tridacna gigas, and Haliotis rufescens sea shells: A comparative study. Mater. Sci. Eng. C 26, 1380–1389.

Mayer, G., Sarikaya, M., 2002. Rigid biological composite materials: Structural examples for biomimetic design. Exper. Mech. 42, 395–403.

Mayer, G., 2005. Rigid biological systems as models for synthetic composites. Science 310, 1144–1147.

Menig, R., Meyers, M.H., Meyers, M.A., Vecchio, K.S., 2000. Quasi-static and dynamic mechanical response of Haliotis rufescens (abalone) shells. Acta Mater. 48, 2383–2398.

Menig, R., Meyers, M.H., Meyers, M.A., Vecchio, K.S., 2001. Quasi-static and dynamic mechanical response of Strombus gigas (conch) shells. Mater. Sci. Eng. A 297, 203–211.

Sarikaya, M., Aksay, J.A., 1992. Nacre of abalone shell; a natural multifunctional nanolaminated ceramic-polymer composite material. In: Case, S. (Ed.), Results and Problems in Cell Differentiation in Biopolymers. Springer, Amsterdam, p. 1.

Sarikaya, M., Gunnison, K.E., Yasrebi, M., Aksay, J.A., 1990. Mechanical property-microstructural relationships in abalone shell. Mater. Res. Soc. 174, 109–116.

Sarikaya, M., 1994. An introduction to biomimetics: A structural viewpoint. Microsc. Res. Tech. 27, 360–375.

Schäffer, T.E., Ionescu-Zanetti, C., Proksch, R., Fritz, M., Walters, D.E., Almqvist, N., Zaremba, C.M., Belcher, A.M., Smith, B.L., Stucky, G.D., Morse, D.E., Hansma, P.K., 1997. Does abalone nacre form by heteroepitaxial nucleation or by growth through mineral bridges? 9, 1731–1740.

Shen, X.Y., Belcher, A.M., Hansma, P.K., Stucky, G.D., Morse, D.E., 1997. Molecular cloning and characterization of lustrin A, a matrix protein from shell and pearl nacre of Haliotis rufescens. J. Biol. Chem. 272, 32472–32481.

Song, F., Soh, A.K., Bai, Y.L., 2003. Structural and mechanical properties of the organic matrix layers of nacre. Biomater 24, 3623–3631.

Song, F., Zhang, X.H., Bai, Y.L., 2002. Microstructure and characteristics in the organic matrix layers of nacre. J. Mater. Res. 17, 1567–1570.

Srinivasan, A.V., Haritos, G.K., Hedberg, F.L., 1991. Biomimetics: Advancing man-made materials through guidance from nature. Appl. Mech. Rev. 44, 463–482.

Su, X.W., Belcher, A.M., Zaremba, C.M., Morse, D.E., Stucky, G.D., Heuer, A.H., 2002. Structural and microstructural characterization of the growth lines and prismatic microarchitecture in red abalone shell and the microstructures of abalone “flat pearls”. Chem. Mater. 14, 3106–3117.

Szilard, R., 2004. Theories and Applications of Plate Analysis. John Wiley & Sons, New Jersey, p. 57.

Ugural, A.C., 1981. Stresses in Plates and Shells. McGraw-Hill, New York, p. 27.

Vincent, J.F.V., 1991. Structural Biomaterials. Princeton University Press, New Jersey.

Wang, R.Z., Suo, Z., Evans, A.G., Yao, N., Aksay, I.A., 2001. Deformation mechanism in nacre. J. Mater. Res. 16, 2485–2493.

Weibull, W., 1951. A statistical distribution function of wide applicability. J. Appl. Mech. 18, 293–297.

Zaremba, C.M., Belcher, A.M., Fritz, M., Li, Y., Mann, S., Hansma, P.K., Morse, D.E., Speck, J.S., Stucky, G.D., 1996. Critical transitions in the biofabrication of abalone shells and flat pearls. Chem. Mater. 8, 679–690.